Boundary slips induced temperature rise and film thickness reduction under sliding/rolling contact in thermal elastohydrodynamic lubrication

Xianghua Meng
Graduate School of Engineering,
Kyushu Institute of Technology,
Fukuoka, 8048550, Japan
xianghua.meng130@mail.kyutech.jp

Jing Wang
College of Mechanical Engineering,
Donghua University,
Shanghai, 201620, China
wj20011226@163.com

Gyoko Nagayama[1]
Department of Mechanical Engineering,
Kyushu Institute of Technology,
Fukuoka, 8048550, Japan
nagayama@mech.kyutech.ac.jp

Abstract:

Temperature rise and film thickness reduction are the most important factors in elastohydrodynamic lubrication (EHL). In the EHL contact area, interfacial resistances (velocity/thermal slips) induced by the molecular interaction between lubricant and solid become significant due to the large surface/volume ratio. Although the velocity slip has been investigated extensively, less attention has been paid on the thermal slip in the EHL regime. In

[1] Corresponding author.
E-mail address: nagayama@mech.kyutech.ac.jp

this study, numerical simulations were conducted by applying three cases of boundary slips to surfaces under sliding/rolling contacts moving in the same direction for the Newtonian thermal EHL. We found that the coupled velocity/thermal slips lead the most significant temperature rise and film thickness reduction among the three cases. The velocity slip results in a lower temperature in the lubricant and solids, whereas the thermal slip causes a temperature rise in the entire contact area in the lubricant as the film thickness decreases simultaneously. Furthermore, the effect of thermal slip on lubrication is more dominant than that of velocity slip while increases the entrainment velocity or slide–roll ratio.

Keywords: Temperature rise; Film thickness reduction; Boundary slips; EHL

1. Introduction

Superlubricity-induced ultralow friction has garnered significant attention owing to its promising prospects of energy saving, environmentally friendly lubrication, and long-life machine operation in industrial applications [1]. To reduce friction in elastohydrodynamic lubrication (EHL) contacts, significant efforts have been expended [2–5]; however, friction reduction caused by the boundary slips between a lubricant and a solid surface is typically accompanied by a significant temperature rise and film thickness reduction in the contact area [6]. From a fundamental perspective, the coupling of the velocity discontinuity [7,8] and temperature jump [9–11] at the solid–lubricant interface are of particular importance for ensuring the lubrication performance in EHL contacts to avoid lubrication breakdown or surface failure.

Over the past decades, boundary slips in EHL have been investigated extensively. The major studies are summarized in Table 1. The lubricant slip effect near the contact surfaces was first reported by Kaneta et al. [12] in 1990. Subsequently, Ehret et al. [13] verified Kanetas' results under different sliding conditions. Fu et al. [14] experimentally demonstrated that an inlet dimple was generated in an EHL film, which was attributed to a velocity slip. Kalin et al. [15] reported that the slip on diamond-like carbon (DLC) coating surfaces resulted in a 20% reduction in the friction coefficient under DLC/DLC contacts compared with that under steel/steel contacts. Guo and Wong et al. [16–18] measured the slip length at a solid surface from the relative movement between an entrapped lubricant and a contact surface. Ponjavic et al. [19,20] performed photobleached imaging to evaluate the effect of interfacial slip on the friction and film thickness in an EHL contact. The velocity slip presented by Wang et al. [21] occurred at a disc surface (that moved faster than the ball surface), which resulted in an anomalous EHL film shape. Under zero entrainment velocity (ZEV) bearing contacts, Wong et al. [22,23] reported a hydrodynamic lubrication film generated by a velocity slip on an oleophobic coating.

In addition to the experimental studies, theoretical models were established to consider the effect of boundary slip on lubrication performance in EHL [24–27, 32–34]. Wen et al. [24] proposed a lubricant ideal viscoplastic rheological model incorporating velocity slip into the line contact without thermal effect. Ståhl et al. [25] and Chu et al. [26] developed slip models for isothermal line contacts. Chen et al. [27] applied an anisotropic velocity slip to a point contact model and discovered a reduction in film thickness in a circular contact. In addition to the friction reduction induced by the boundary slips, the temperature rise induced via heat generation from the lubricant can lower friction owing to the reduction in the lubricant viscosity in the EHL contact. Consequently, temperature rise in the contact regime is an indispensable factor in tribology [28–31]. Zhao et al. [32] found that the velocity slip reduced temperature rise and increased the film thickness owing to the positive effect of lubricant entrainment under large slide–roll ratios (SRRs). Zhang et al. [33,34] proposed a layered oil slip lubrication model that included the thermal effect of the EHL point contact under various operation conditions.

Although the effect of velocity slip on lubrication performance has been investigated extensively, the thermal slip and the coupled velocity/thermal slips have rarely been considered in the EHL regime. Related studies on the thermal slip were summarized in Table 2. Due to the difficulties in measurement of thermal slip, various advanced techniques have been applied to the experimental systems including the solid–liquid interface. Despite the fact that great efforts have been devoted to the measurement, it is still a challenging work to evaluate the thermal slip at the solid–liquid interface experimentally. On the other hand, with the aid of molecular dynamics simulation, the thermal slip at the solid–liquid interface has been extensively investigated. The thermal slip length (i.e., Kapitza length) at the hydrophilic solid–liquid interface is qualitatively smaller than that at the hydrophobic solid–liquid interface.

In the EHL contact area, interfacial resistances (velocity/thermal slips) induced by the molecular interaction between lubricant and solid become significant due to the large surface/volume ratio. That is, the boundary slips can no longer be ignored when the slip length or thermal slip length is comparable to the characteristic film thickness. In our previous study, we applied velocity and thermal slips to one of the sliding/rolling surfaces in ZEV contact; however, less attention has been paid on the temperature rise and the film thickness reduction [6]. Since boundary slips may occur at all moving surfaces in practical EHL, we conducted a further thermal EHL analysis in this study by applying boundary slip conditions to two moving surfaces under sliding/rolling contacts in the same direction. Three cases of boundary slips, i.e., velocity, thermal, and coupled velocity/thermal slips, were investigated to clarify the phenomena of temperature rise and film thickness reduction in thermal EHL. The adopted boundary slips length is comparable to the typical film thickness of the EHL contact.

Table 1 Review of EHL studies on velocity slip.

Year	Authors	Method/findings	Ref.
Experimental studies			
1990	Kaneta et al.	Ball-disc under pure rolling and sliding contact / velocity slip at or near contact surfaces	[12]
2007	Fu et al.	Ball-disc under pure sliding contact with high viscosity polymeric lubricant / velocity slip induced inlet dimple in contact region	[14]
2009	Kalin et al.	DLC-DLC contacts / 20% friction reduction compared to steel-steel contact	[15]
2012	Guo et al.	Entrapped lubricant in ball-disc contact / slip length of 0–12 μm at steel-lubricant (PB900/PB1300)-glass surfaces	[16]
2014	Ponjavic et al.	Glass-Fusso contact in PCS Instruments / central film thickness reduction of 50% due to velocity slip at Fusso coating surface	[19,20]
2017	Wang et al.	Ball-disc contact lubricated by 1-dodecanol / anomalous EHL film caused by velocity slip	[21]
2018	Wong et al.	ZEV contact with oleophobic coating / hydrodynamic lubrication film due to velocity slip at oleophobic surface	[22,23]
Theoretical analysis			
2000	Wen et al.	Isothermal line contact, viscoplastic rheological model / velocity slip occurred at the inlet zone	[24]
2003	Ståhl et al.	Line contact, limiting shear stress / central film thickness variations due to velocity slip	[25]
2012	Chu et al.	Line contact, Navier-slip and flow rheology / correlation between slip length and film thickness	[26]
2016	Chen et al.	Circular contact, anisotropic slip / film thickness reduction due to slip length in sliding direction	[27]
2019	Zhao et al.	Point contact, SRR = 44, velocity slips at two surfaces / variations of temperature rise and film thickness	[32]
2020	Zhang et al.	Point contact, layered oil slip model / reduction of film thickness due to velocity slip and thermal effect	[33,34]
2021	Meng et al.	Point contact, boundary slips at one of moving surfaces / film thickness reduction and temperature rise in contact region	[6]

Table 2 Recent studies on thermal slip at solid–liquid interface.

Year	Authors	Method/findings	Ref.
Experimental studies			
2006	Ge et al.	Time-domain thermoreflectance / water–Au interface, l_k = 3–6 nm at hydrophilic interfaces, l_k = 10–12 nm at hydrophobic interfaces	[35]
2010	Timofeeva et al.	Transient hot wire method / water–α-SiC interface, $l_k \approx 4.2 \pm 0.3$ nm	[36]
2017	Nagayama et al.	Forced convection in fully developed microchannel flow / water–Si interface, l_k = 50–150 μm	[37]
Molecular dynamics studies			
2010	Nagayama et al.	Nonequilibrium molecular dynamics simulations / Pt–Ar nanostructured interface, l_k = 3.4 – 9.8 nm at hydrophilic surface, l_k = 16.4 – 51.6 nm at hydrophobic surface	[38]
2012	Hu et al.	Molecular dynamics simulations using LAMMPS / water–gold interface, $l_k \approx 2 – 5$ nm	[39]
2012	Shi et al.	Molecular dynamics simulations using LAMMPS / l_k = 0 – 1.2 nm at Ar–silver interface, l_k = 3.1 – 3.5 nm at Ar–graphite interface	[40]
2014	Barisik et al.	Molecular dynamics simulations using LAMMPS / water–Si interface, $l_k \approx 8.5 – 9$ nm	[41]
2016	Pham et al.	Molecular dynamics simulations using LAMMPS / water and graphene-coated-Cu (111) interface, l_k = 10 – 50 nm	[42]
2021	Song et al.	Molecular dynamics simulations using LAMMPS / Ar–Cu interface, l_k = 0–14 nm in rough nanochannels	[43]

2. Method

A steel–steel configuration comprising a disc (solid a) and a ball (solid b) was employed as a stationary EHL point contact subjected to an external load w, as shown in Fig. 1(a). The velocities of the disc and ball are u_a and u_b in the x-direction, respectively. Fig. 1(b) shows the corresponding computational domain $-5a \le x \le 5a$, $-5a \le y \le 5a$, $-5a \le z \le 5a + h$, where a is the half Hertzian contact width, and h is the lubricant film thickness. The origin of coordinate system o is located at the center of the contact area. Five grid levels were employed in the computational domain. In the x- and y-directions, 256 equidistant nodes were adopted at the finest level, whereas in the z-direction, 11 equidistant nodes were adopted in the lubricant film and 12 non-equidistant nodes in the solids. Table 3 lists the operating conditions used in this study.

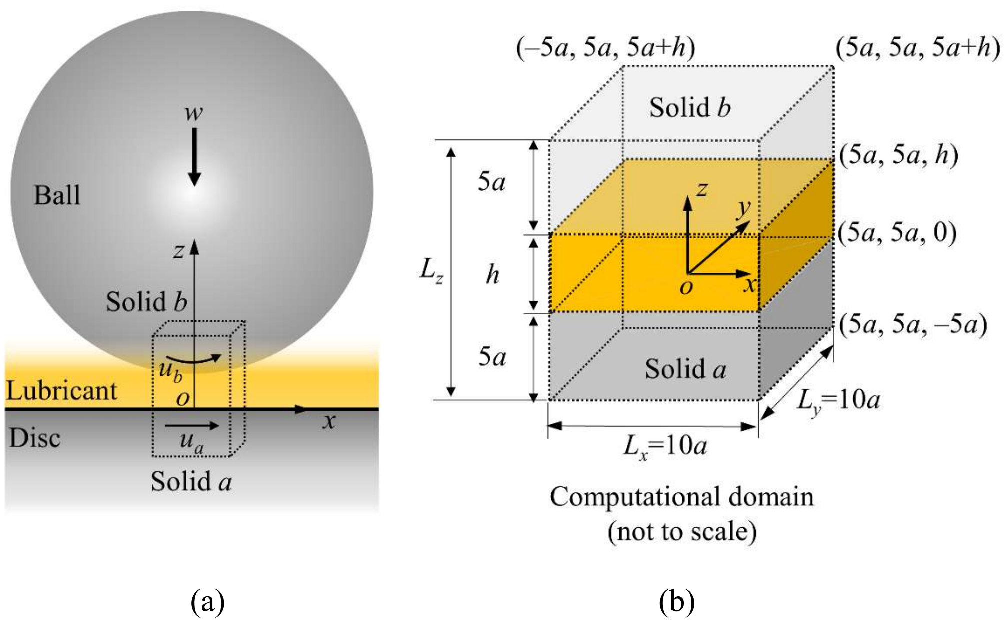

Fig. 1 Schematic illustrations of (a) sliding/rolling contact, and (b) computational domain (not to scale)

Table 3 Operating conditions

Ambient temperature, T_0, K	313
Ball radius, R, m	0.0127
Load, w, N	30
Half width of Hertzian contact, a, μm	136
Entrainment velocity, $u_e = (u_a + u_b)/2$, m/s	0 – 30
Slide-roll ratio, SRR = $(u_a - u_b)/u_e$	0 – 2

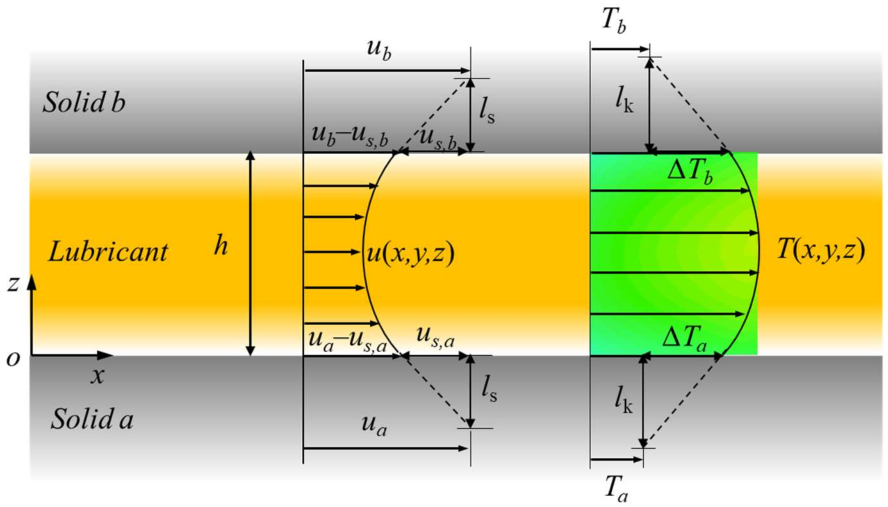

Fig. 2 Boundary slips at surfaces of moving solids: velocity slip (left) and thermal slip (right)

The lubrication performances were investigated by solving the Reynolds equation and energy equations under the boundary slips condition shown in Fig. 2. Since the lubricant is assumed to be the isotropic Newtonian fluid in this study, the linear relation between the shear strain rate and shear stress is considered. In contrast to our previous study [6], both the surfaces of solids a and b were assumed to be subjected to the same boundary slips. The linear Navier slip condition [7,8] and Kapitza resistance [9,10] were adopted for the slip velocity and temperature jump, as illustrated in Fig. 2, where l_s is the slip length and l_k is the thermal slip length. Hence, the lubricant velocity and temperature at the solid–lubricant interfaces are applied as follows:

$$\begin{cases} u_{z=0} = u_a - l_s \left.\dfrac{\partial u}{\partial z}\right|_{z=0} \\ u_{z=h} = u_b + l_s \left.\dfrac{\partial u}{\partial z}\right|_{z=h} \end{cases} \tag{1}$$

$$\begin{cases} T_{z=0} = T_a + l_k \left.\dfrac{\partial T}{\partial z}\right|_{z=0} \\ T_{z=h} = T_b - l_k \left.\dfrac{\partial T}{\partial z}\right|_{z=h} \end{cases} \tag{2}$$

By applying the lubricant velocity at the interfaces (specified in Eq. (1)) to the Reynolds equation, a modified Reynolds equation is obtained.

$$\frac{\partial}{\partial x}\left[\left(\frac{\rho}{\eta}\right)_{es} h^3 \frac{\partial p}{\partial x}\right] + \frac{\partial}{\partial x}\left[\left(\frac{\rho}{\eta}\right)_{e} h^3 \frac{\partial p}{\partial x}\right] + \frac{\partial}{\partial y}\left[\left(\frac{\rho}{\eta}\right)_{e} h^3 \frac{\partial p}{\partial y}\right] = 6\left(u_a + u_b\right)\frac{\partial \rho^* h}{\partial x} \tag{3}$$

where $\left(\dfrac{\rho}{\eta}\right)_{es} = 12\left[l_s \dfrac{B}{A}\dfrac{\rho_e}{h^2} + \left(\dfrac{B}{A}\dfrac{\eta_{z=0}}{h} - \dfrac{\eta_e}{\eta_e'}\right)\rho_e'\right]$, $\left(\dfrac{\rho}{\eta}\right)_{e} = 12\left(\dfrac{\eta_e}{\eta_e'}\rho_e' - \rho_e''\right)$,

$A = h\eta_{z=0}\eta_{z=h} + l_s\eta_e\left(\eta_{z=h} - \eta_{z=0}\right)$, $B = h^2\left(\dfrac{\eta_e}{\eta_e'}\right)\eta_{z=h} - l_s\eta_e h$, $\eta_e = h \Big/ \displaystyle\int_0^h \frac{1}{\eta}dz$,

$\eta_e' = h^2 \Big/ \displaystyle\int_0^h \frac{z}{\eta}dz$, $\rho_e = h^{-1}\displaystyle\int_0^h \rho dz$, $\rho_e' = h^{-2}\displaystyle\int_0^h \rho \int_0^z \frac{1}{\eta}dz'dz$, $\rho_e'' = h^{-3}\displaystyle\int_0^h \rho \int_0^z \frac{z'}{\eta}dz'dz$,

$\rho^* = \dfrac{2}{u_a + u_b}\left[u_a\rho_e - \left(u_a - u_b\right)\eta_e\rho_e'\rho_{es}\right]$, $\rho_{es} = \dfrac{\eta_{z=h}}{A}\left(l_s\dfrac{\rho_e}{\rho_e'} + h\eta_{z=0}\right)$.

Eq. (3) coincides with the Reynolds equation [44] under the no-slip boundary condition, where the slip parameters are $(\rho/\eta)_{es} = 0$ and $\rho_{es} = 1$. To obtain the temperature profiles of the system, the full energy equations in the lubricant film and contacting solids were solved by considering the heat generated by the shearing and compression of the lubricant.

To resolve the local temperature filed, the full energy equations within the lubricant film and solids are described. Within the lubricant film, the energy equation [45] is expressed as

$$c\left(\rho u\frac{\partial T}{\partial x}+\rho v\frac{\partial T}{\partial y}-q\frac{\partial T}{\partial z}\right)-k\frac{\partial^2 T}{\partial z^2} = -\frac{T}{\rho}\frac{\partial \rho}{\partial T}\left(u\frac{\partial p}{\partial x}+v\frac{\partial p}{\partial y}\right)+\eta\left[\left(\frac{\partial u}{\partial z}\right)^2+\left(\frac{\partial v}{\partial z}\right)^2\right] \tag{4}$$

Within the solids, no compression and shearing are present, the energy equation for solids are written as:

$$\begin{cases} c_a\rho_a u_a\dfrac{\partial T}{\partial x}=k_a\left(\dfrac{\partial^2 T}{\partial z_a^2}+\dfrac{\partial^2 T}{\partial x^2}+\dfrac{\partial^2 T}{\partial y^2}\right) \\ c_b\rho_b u_b\dfrac{\partial T}{\partial x}=k_b\left(\dfrac{\partial^2 T}{\partial z_a^2}+\dfrac{\partial^2 T}{\partial x^2}+\dfrac{\partial^2 T}{\partial y^2}\right) \end{cases} \tag{5}$$

The relevant properties of the lubricant and steel are listed in Table 4. The Dowson and Higginson model [46] and the Roelands equation [47] were applied to estimate the density and viscosity of the lubricant as functions of pressure and temperature, as follows:

$$\rho=\rho_0\left[1+\frac{0.6\times10^{-9}p}{1+1.7\times10^{-9}p}-0.00065\left(T-T_0\right)\right] \tag{6}$$

$$\eta=\eta_0\exp\left\{\left(\ln\eta_0+9.67\right)\left[-1+\left(1+5.1\times10^{-9}p\right)^{Z_0}\left(\frac{T-138}{T_0-138}\right)^{-S_0}\right]\right\} \tag{7}$$

Here, ρ_0 is the density, η_0 is the viscosity of the lubricant at $p = 0$ and $T = T_0$, Z_0 is the pressure–viscosity index, and S_0 is the temperature–viscosity index. Although the low thermal conductivity of steel would cause a temperature rise in the EHL contact [48–50], for simplicity, the steel thermal conductivity is set to 46 W/(m·K) in this study.

The simulation involved two procedures: (1) solving Eq. (3) under the fixed temperature field by applying the multilevel, multi-integration technique and multigrid method [51]; (2) solving the energy equations under the fixed pressure field (obtained from step (1)) by employing the sequential column sweeping method [52]. These procedures were repeated until the relative errors of pressure, load, and temperature were less than 1×10^{-3}, 1×10^{-3}, and 1×10^{-4}, respectively [6].

Table 4 Properties of lubricant and steel

Density of steel, $\rho_{a,b}$, kg/m^3	7850
Specific heat of steel, $c_{a,b}$, J/(kg·K)	470
Thermal conductivity of steel, $k_{a,b}$, W/(m·K)	46
Ambient density of lubricant, ρ_0, kg/m^3	875
Specific heat of lubricant, c, J/(kg·K)	2000
Thermal conductivity of lubricant, k, W/(m·K)	0.14
Pressure viscosity coefficient, α, 1/Pa	2.4×10^{-8}
Ambient viscosity of lubricant, η_0, Pa·s	0.08
Thermal viscosity coefficient of lubricant, β, 1/K	0.042
Reduced elastic modules, E', Pa	2.26×10^{11}

3. Results and discussion

3.1 Lubrication with boundary slips

To characterize the effects of boundary slip on lubrication, three cases of boundary slips were investigated in our numerical simulations: (1) velocity slip, (2) thermal slip, and (3) coupled velocity/thermal slips; subsequently, these cases were compared with the classical no-slip solution. Figs. 3–6 show the typical results obtained under $u_e = 3.6$ m/s and SRR = 1.5. In the current study, $-1 \leq X = x/a \leq 1$ and $-1 \leq Y = y/a \leq 1$ correspond to the area of the Hertzian contact, and $X = Y = 0$ corresponds to the center of the contact area.

The contour maps of the film thickness, pressure, and film thickness profiles are shown in Fig. 3. Here, the boundary slips length of 0.2 μm is adopted in this section, which is comparable to the typical film thickness of the EHL contact [53]. The result of $l_s = l_k = 0$, which is a typical solution of the EHL point contact, is shown in Fig. 3(a). A central plateau and an outer constriction are evident in the contour maps. Compared with Fig. 3(a), a greater pressure peak is shown in Fig. 3(b), whereas lower pressure peaks are shown in Figs. 3(c) and 3(d). Meanwhile, the film thickness at the outer constrictions decreases when $l_s = 0.2$ μm and $l_k = 0$, as shown in Fig. 3(b), whereas the central plateau film inclines slightly when $l_s = 0$ and $l_k = 0.2$ μm, as shown in Fig. 3(c). For the coupled velocity/thermal slips when $l_s = l_k = 0.2$ μm, as shown in Fig. 3(d), the film thickness at the outer constrictions decreases, accompanied by an inclined lubricant film. The film thickness shown in Fig. 3(d) is the thinnest among the cases, owing to the reduction in film thickness induced by the velocity slip and thermal slip. The film thickness reduction induced by the velocity slip is attributed to the lower lubricant velocity, which entrains less lubricant into the contact area [6,54]. On the other hand, the thermal slip-induced film thickness reduction is attributed to the lower viscosity of the lubricant due to the temperature rise in the contact area. Comparing the minimum film thickness with that of the no-slip (dotted line) and $l_s = l_k = 0.2$ μm (dashed line) cases, it is clear that the film thickness reduction is primarily induced by the velocity slip.

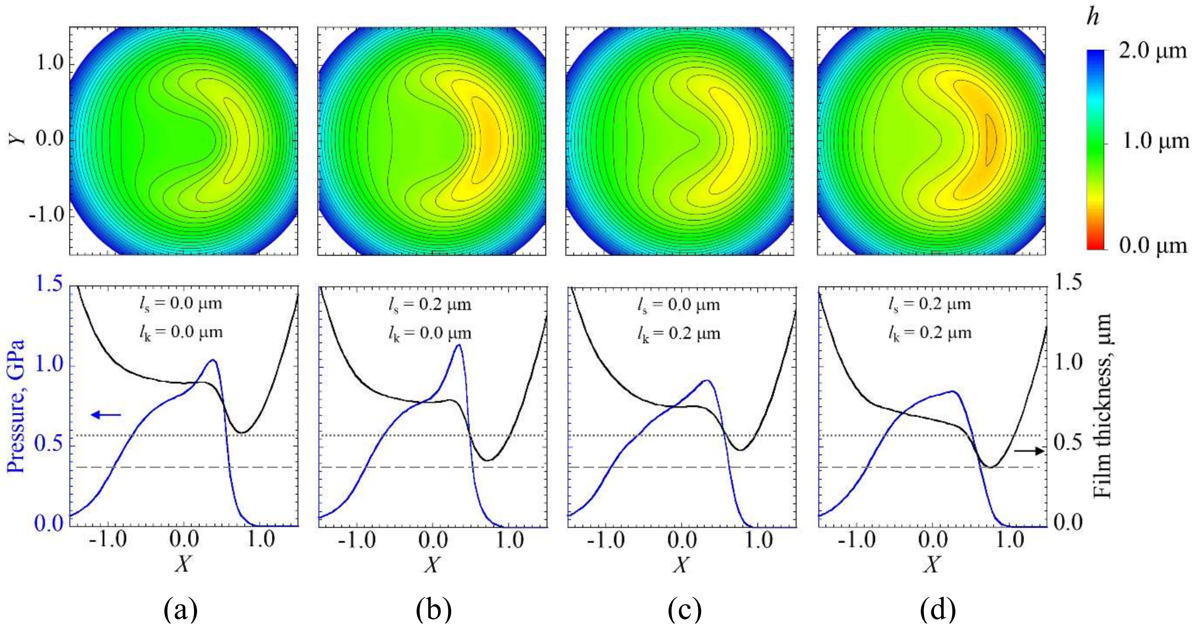

Fig. 3 Contour maps of film thickness (top) and pressure, film thickness profiles on center plane $Y = 0$ (bottom) at $u_e = 3.6$ m/s, SRR = 1.5 under different boundary conditions: (a) no slip;

(b) velocity slip; (c) thermal slip; (d) coupled velocity/thermal slips. Dotted line represents minimum film thickness of no-slip case; dashed line represents minimum film thickness for case of $l_s = l_k = 0.2$ μm

Fig. 4 presents the temperature profiles on the center plane ($Y = 0$) in the EHL contact area. Fig. 4(a) shows the results of the no-slip boundary condition ($l_s = l_k = 0$), where the temperature of the lubricant increases significantly at the center of the film thickness. This temperature rise is caused by the heat generated in the lubricant film due to the compression and shearing in the EHL contact area. Since the generated heat can be removed from the lubricant to the two moving solid walls, increasing the wall velocity can enhance heat dissipation. Consequently, both the surface temperature and the inner temperature of solid *a* are smaller than those of solid *b* because the velocity of solid *a* is seven times larger than that of solid *b* at SRR = 1.5. In the case of $l_s = 0.2$ μm, the temperature profile in Fig. 4(b) is similar to that in Fig. 4(a), but the maximum lubricant temperature is higher than that in Fig. 4(a) because of the increase in the maximum pressure under velocity slip. Comparing Figs. 4(c) and 4(d) to 4(a), the area of lubricant temperature exceeding 400 K (green) expands significantly at the left side of the contact area, whereas the maximum lubricant temperature decreases. In particular, the lubricant temperature near the solid walls increases significantly. The main reason for this temperature rise is the limited heat dissipation from the lubricant to solids under thermal slip at the two moving solid boundaries. Therefore, the temperature rises in solids *a* and *b* shown in Figs. 4(c) and 4(d) are undistinguishable compared with those in Figs. 4(a) and 4(b). Meanwhile, since a higher lubricant temperature results in a lower viscosity, thinner film thicknesses are formed in Figs. 4(c) and 4(d) compared with those shown in Fig. 4(a). However, the film thickness reduction induced by the thermal slip is smaller than that induced by the velocity slip. In other words, when the thermal slip length is the same as the slip length, the film thickness reduction is primarily induced by the velocity slip, as described previously.

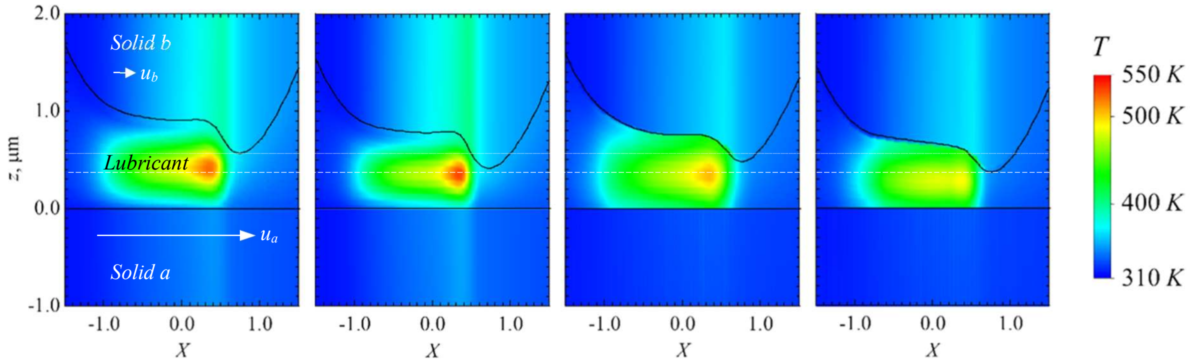

(a) (b) (c) (d)

Fig. 4 Temperature profiles on center plane ($Y = 0$) in EHL contact area at $u_e = 3.6$ m/s, SRR = 1.5 under different boundary conditions: (a) $l_s = l_k = 0$; (b) $l_s = 0.2$ μm, $l_k = 0$; (c) $l_s = 0$, $l_k = 0.2$ μm; (d) $l_s = l_k = 0.2$ μm. Dotted line represents minimum film thickness of (a); dashed line represents minimum film thickness of (d)

The results presented in Figs. 3 and 4 show that the coupled velocity/thermal slips exhibit the worst tribological performance among the cases investigated. In particular, the effect of thermal slip on the temperature rise in the vicinity of the solid walls is dominant. Since the thermal slip length might not be of the same order as the slip length [37,55], further analysis was conducted to investigate the superiority of the boundary slips.

Figs. 5–6 show the results under the coupled velocity/thermal slips, where the cases of $l_s / l_k < 1$ indicate the superiority of thermal slip over velocity slip, and those of $l_s / l_k > 1$ indicate the superiority of velocity slip over thermal slip. Similar to Fig. 3, the contour maps of the lubricant film thickness (top), centerline profiles of film thickness, and pressure (bottom) are shown in Fig. 5. As shown in the contour maps, the film thickness at the center plateau and outer constriction decreases with the increase in the thermal slip length (Figs. 5(a)–5(c)) or velocity slip length (Figs. 5(d), 5(e)). The film thickness reduction shown in Figs. 5(c) and 5(e) is more significant than that of the other cases, where a thin lubricant film of 20–60 nm covers the entire EHL contact area. Meanwhile, the pressure peak shown in Figs. 5(c) and 5(e) are less evident compared with those shown in Figs. 5(a) and 5(d). A further increase in the boundary slips might result in a transition from EHL to boundary lubrication, accompanied by lubrication failure at the contact area. In the case of $l_s / l_k < 1$, the film thickness reductions are dominated by thermal slip, whereas those of $l_s / l_k > 1$ are due to the superiority of the velocity slip.

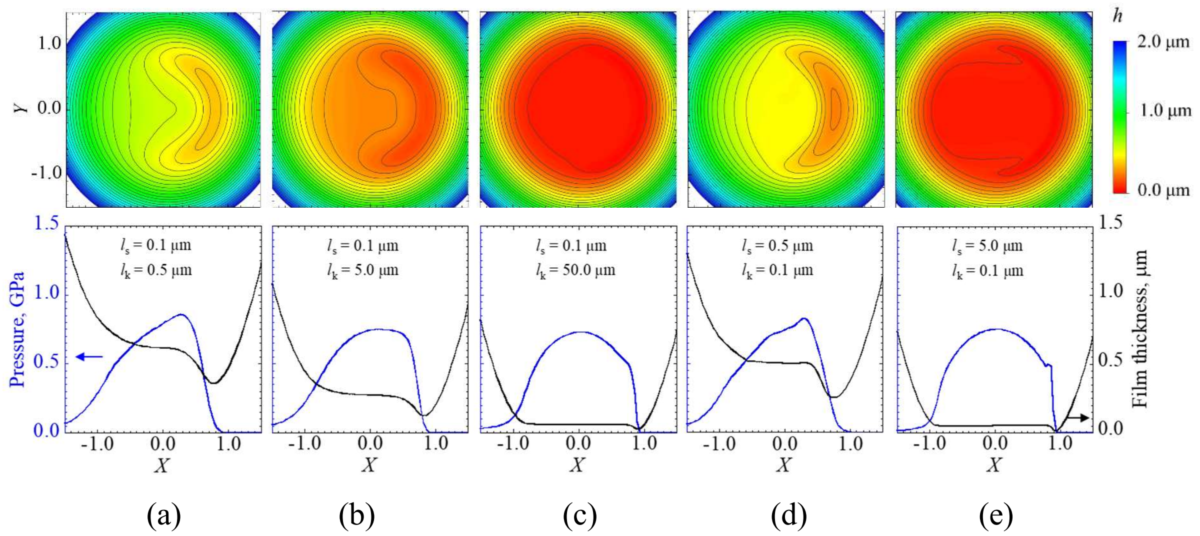

Fig. 5 Contour maps of film thickness (top) and pressure. Film profiles on center plane Y = 0 (bottom) at u_e = 3.6 m/s, SRR = 1.5 under coupled velocity/thermal slips: (a) l_s / l_k = 0.1 μm/ 0.5 μm; (b) l_s / l_k = 0.1 μm/ 5.0 μm; (c) l_s / l_k = 0.1 μm/ 50.0 μm; (d) l_s / l_k = 0.5 μm/ 0.1 μm; (e) l_s / l_k = 5.0 μm/ 0.1 μm

Similar to Fig. 4, Fig. 6 shows the temperature profiles under the coupled velocity/thermal slips; Figs. 6(a)–6(c) show the cases of $l_s / l_k < 1$, whereas Figs. 6(d) and 6(e) show the cases of $l_s / l_k > 1$. As shown in Figs. 6(a)–6(c), a larger l_k induces a more significant lubricant temperature rise in the entire contact area. The reason contributing to the l_k-induced temperature rise is the same as that for Fig. 4, i.e., the limited heat dissipation from the lubricant to the solids. The maximum lubricant temperature rise is approximately 300 K at l_k = 50.0 μm, as shown in

Fig. 6(c), accompanied by a temperature rise in the entire contact area of the lubricant. Simultaneously, the lubricant film thickness decreases to a critical level owing to the reduced viscosity corresponding to the temperature rise. Meanwhile, the larger l_s induces a lower lubricant temperature rise, as shown in Figs. 6(d) and 6(e). Since the lubricant velocity decreases under the velocity slip, the amount of heat generation decreases and hence, a smaller temperature rise is induced in the contact area. Meanwhile, the lower lubricant velocity limits the amount of lubricant entraining into the contact area and hence, reduces the film thickness.

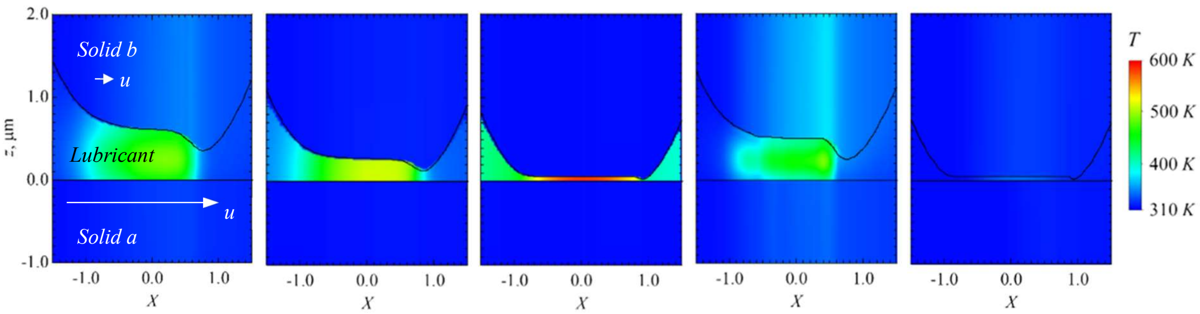

(a) (b) (c) (d) (e)

Fig. 6 Temperature profiles in EHL contact area on center plane $Y = 0$ at u_e = 3.6 m/s and SRR = 1.5 under coupled velocity/thermal slips: (a) l_s / l_k = 0.1 μm/ 0.5 μm; (b) l_s / l_k = 0.1 μm/ 5.0 μm; (c) l_s / l_k = 0.1 μm/ 50.0 μm; (d) l_s / l_k = 0.5 μm/ 0.1 μm; (e) l_s / l_k = 5.0 μm/ 0.1 μm

In summary, the velocity slip dominates the film thickness reduction when the slip length is comparable to the thermal slip length, whereas the thermal slip dominates the film thickness reduction when the slip length is negligible compared with the thermal slip length. In the coupled velocity/thermal slips case, the superior velocity slip might result in a lower temperature in the lubricant and solids, whereas the superior thermal slip might result in a temperature rise in the entire contact area in the lubricant as the film thickness decreases simultaneously.

3.2 Effects of entrainment velocity on lubrication with boundary slips at a specified SRR

The entrainment velocity is known as one of the key parameters in the lubrication of sliding/rolling contacts because the entrainment velocity can result in a variation in the amount of entrained lubricant and shear rate. Hence, the effects of the entrainment velocity on the lubrication characteristics with boundary slips at SRR = 1.5 are discussed in this section.

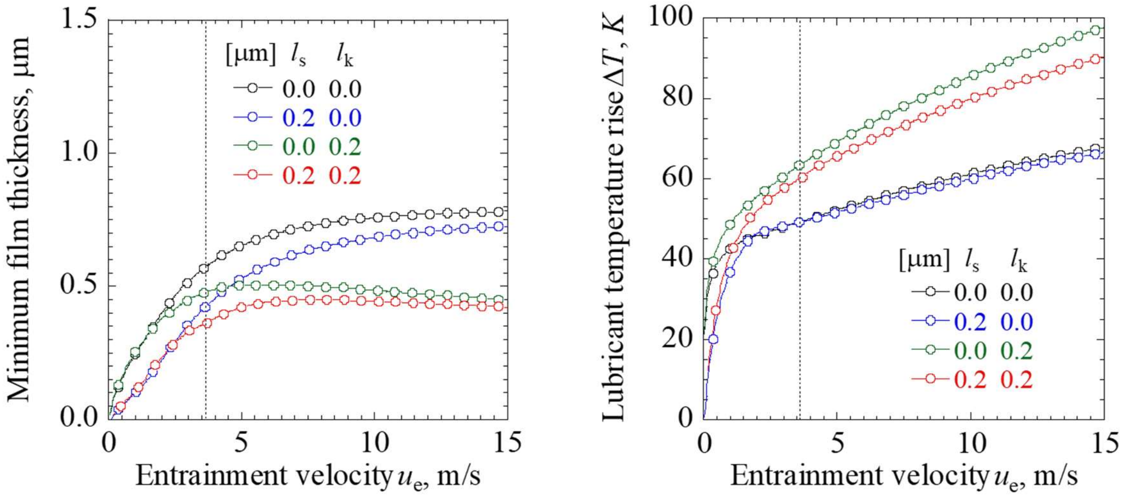

(a) (b)

Fig. 7 Effect of entrainment velocity on lubrication performance at SRR = 1.5: (a) minimum film thickness; (b) mean lubricant temperature rise in entire contact area. Dashed line corresponds to u_e = 3.6 m/s applied in Figs. 3–4

Fig. 7 shows the minimum film thickness and mean lubricant temperature rise curves with the entrainment velocity under boundary slips, where ΔT is the average value of the lubricant temperature rise over the entire contact area. The dashed line corresponds to u_e = 3.6 m/s applied in Figs. 3 and 4. In the low entrainment velocity region of u_e < 3 m/s, the minimum film thickness of the no-slip case (black) is consistent with that of the thermal slip case (green) because of the insignificant temperature rise, whereas those of the cases with velocity slips (blue and red) are relatively smaller. Therefore, the minimum film thickness reduction is primarily caused by velocity slip. When the entrainment velocity increases, the minimum film thickness reduction caused by the velocity slip (blue) decreases; however, that caused by the thermal slip (green and red) increases. With an increase in the entrainment velocity, the amount of entrained lubricant in the contact area increases, which facilitates the increase in the film thickness. By contrast, heat generation increases owing to increased lubricant shearing, resulting in a reduction in the film thickness. The contributions of velocity and thermal slips to the minimum film thickness reduction are equal at u_e = 4.6 m/s. Meanwhile, an apparent discrepancy appears in the cases with and without thermal slip in the high entrainment velocity region. The reason is shown Fig. 7(b), where the temperature rise is significant in the cases with thermal slip, which results in the apparent discrepancy in the minimum film thicknesses in the high entrainment velocity region.

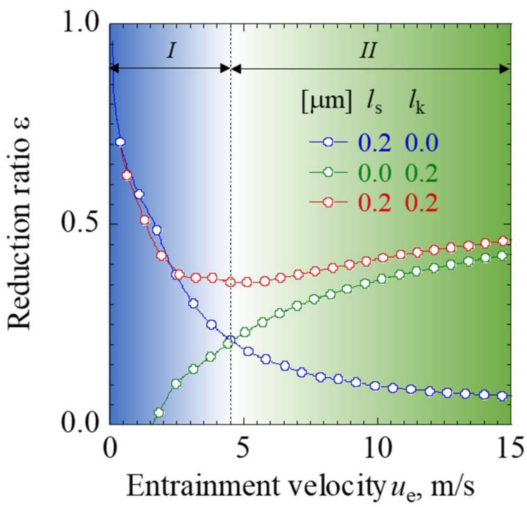

Fig. 8 Reduction ratio of minimum film thickness ε vs. entrainment velocity curves at SRR = 1.5. Dashed line represents threshold between regions *I* and *II*

To compare the effects of boundary slips on the minimum film thickness, the ratio of the minimum film thickness reduction is plotted as a function of the entrainment velocity, as show in Fig. 8. The ratio of the minimum film thickness reduction ε is defined as ε = $(h_{min0} - h_{min}) / h_{min0}$, where h_{min0} is the minimum film thickness under the no-slip boundary condition. As shown in Fig. 8, at u_e = 4.6 m/s, the ε of the velocity slip case (blue) is equal to that of the thermal slip case (green), whereas that of the coupled velocity/thermal slips case (red) shows the minimum value. This implies that in region I of u_e < 4.6 m/s, velocity slip dominates the minimum film thickness reduction. By contrast, in region II of u_e > 4.6 m/s, the effect of thermal slip on ε is more dominant than that of velocity slip.

3.3 Effects of SRR on lubrication with boundary slips at specified entrainment velocity

Since the lubricant temperature rise is induced by the lubricant shearing with regard to the lubricant shear rate or the relative velocity between solids a and b in the EHL contact, the effects of SRR on the lubrication characteristics are discussed in this section.

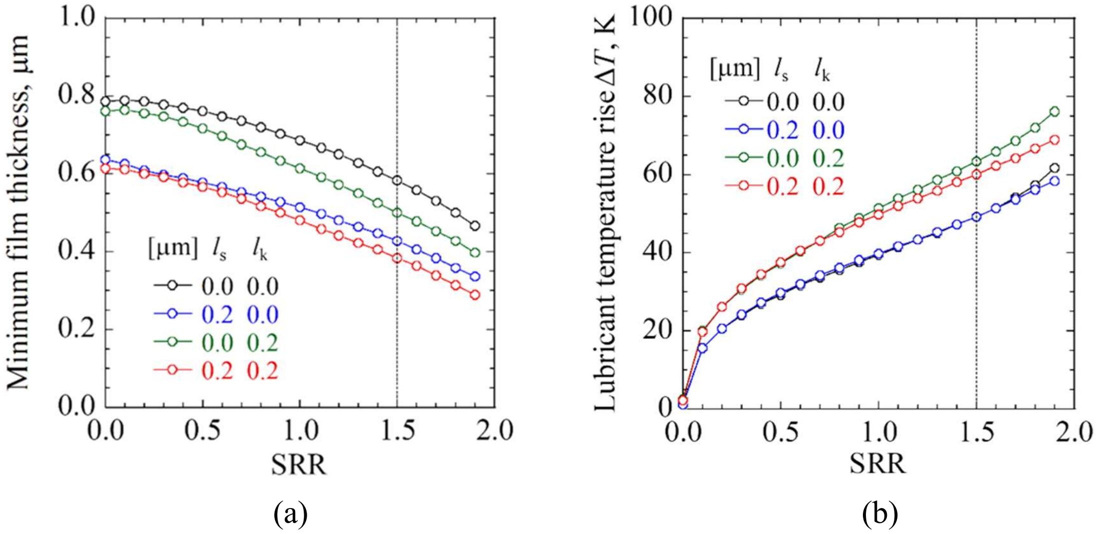

Fig. 9 Effect of SRR on lubrication performance at u_e = 3.6 m/s: (a) minimum film thickness; (b) mean lubricant temperature rise in entire contact area

Figs. 9(a) and 9(b) show the variations in the minimum film thickness and lubricant temperature rise with boundary slips. The entrainment velocity is given as u_e = 3.6 m/s. The dashed line denotes SRR = 1.5, corresponding to the results shown in Figs. 3 and 4. It is clear that increasing the SRR reduces the minimum film thickness but increases in the temperature rise. As shown in Fig. 9(a), the thermal slip has less significant effect than the velocity slip on the minimum film thickness reduction, whereas the velocity slip yields a significant minimum film thickness reduction of approximately 0.15 μm. Meanwhile, the film thickness reduction of the coupled velocity/thermal slips is dominated by the velocity slip in the low SRR region, whereas the effect of the thermal slip on the film thickness reduction become more prominent in the large SRR region. As discussed previously in Section 3.1, the film thickness reduction is caused by two reasons: (1) the lower lubricant velocity induced by the velocity slip, and (2) the lower viscosity induced by the thermal slip. The latter coincides with the temperature rise in the entire contact area, which increases with the SRR, as shown in Fig. 9(b). Hence, the film thickness reduction in the case of coupled velocity/thermal slips is the largest among the cases investigated.

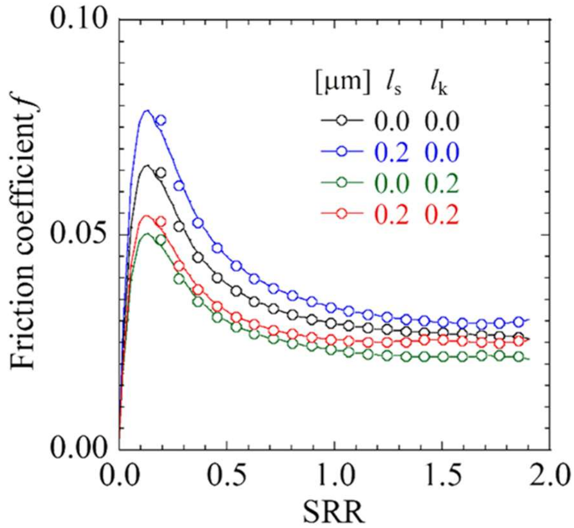

Fig. 10 Friction coefficient vs. SRR curves at u_e = 3.6 m/s

Fig. 10 shows the f-SRR curves at u_e = 3.6 m/s, where f is the friction coefficient. As shown, a greater velocity slip results in a higher f, whereas a greater thermal slip results in a lower f. The former is caused by the film thickness reduction subjected to a large velocity gradient, whereas the latter is caused by the reduction in lubricant viscosity due to a temperature rise.

Although the trend of the f-SRR curves is consistent with the experiments presented in [1,56], the operating conditions for those experiments are not comparable to those used in the present study. To date, only a few experimental results reported are comparable to simulation results or theoretical predictions. In Fig. 11, for illustrative purposes, the experimental results of glycerol/steel contact [1] are compared with the simulation results using the same operating conditions reported in [1]. The simulation results under the no-slip condition of $l_s = l_k = 0$ are consistent with the experimental results for the uncoated substrates, whereas those under the coupled slips of $l_s = 0.05$ μm and $l_k = 0.6$ μm are consistent with the experiments of DLC-coated substrates. Here, the thermal slip length for the DLC-coated surface [1] is estimated to 0.6 μm, including both the effects of the DLC coating and the interfacial thermal resistance. Since the DLC coating is 2.8 μm in thickness and its thermal conductivity is 2 W/(m·K), the thermal resistant of the coating layer is 1.4×10-6 K/W. This is 2 orders of magnitude smaller than that of equivalent interfacial thermal resistance (approximately 1.2×10^{-4} K/W), Therefore, the estimated thermal slip length l_k = 0.6 μm principally attributes to the interfacial thermal resistance. Accordingly, the deviations of the experimental results between the uncoated and DLC-coated substrates are significant, which imply that the boundary slips are of great importance to the superlubricity.

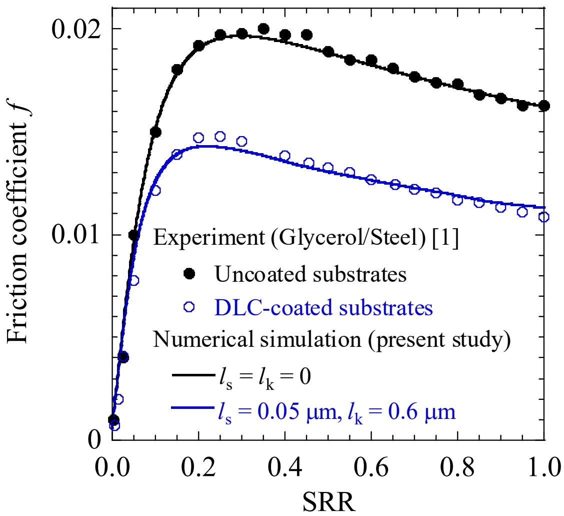

Fig. 11 Comparisons of f-SRR curve between experiments [1] and numerical simulations at u_e = 1.6 m/s and w = 300 N

The quantitative estimation of the slip length and thermal slip length is crucial for providing a fundamental understanding of solid–lubricant interfaces for applications in superlubricity, albeit challenging. The method proposed herein facilitates the design and innovation of next-generation tribological technology.

4. Conclusion

Temperature rise and film thickness reduction were investigated via numerical simulations of thermal EHL under slip boundary conditions. Three cases of boundary slips, velocity, thermal, and coupled velocity/thermal slips, were applied to surfaces under sliding/rolling contacts moving in the same direction, and the following conclusions were obtained:

(1) The velocity slip dominates the film thickness reduction when the slip length is comparable to the thermal slip length, whereas the thermal slip dominates the film thickness reduction when the slip length is negligible compared with the thermal slip length. In the coupled velocity/thermal slips case, the superior velocity slip might result in a lower temperature in the lubricant and solids, whereas the superior thermal slip might cause a temperature rise in the entire contact area in the lubricant as the film thickness decreases simultaneously. Hence, the coupled velocity/thermal slips case leads the most significant temperature rise and film thickness reduction among the three cases.

(2) The effect of thermal slip on lubrication is more dominant than that of velocity slip while increase entrainment velocity or SRR. At the critical entrainment velocity, the coupled velocity/thermal slips case has the minimum film thickness reduction ratio, which can improve the tribological performance.

(3) The slip length and thermal slip length are estimated to be l_s = 0.05 μm and l_k = 0.6 μm on the DLC-coated surface based on the experimental data in [1].

The proposed method for estimating the slip length and thermal slip length quantitatively is challenging but beneficial for gaining a fundamental understanding of superlubrication. Further experimental investigations are necessary to verify the results obtained.

Acknowledgment

This work is partly supported by the Ministry of Education, Science and Culture of the Japanese Government through the Grant-in Aid for Scientific Research, Project No. 18H01385, National Natural Science Foundation of China, No. 51275253 and the Initiative for Realizing Diversity in the Research Environment by Ministry of Education, Culture, Sports, Science and Technology, Japan.

References

[1] Björling, M., and Shi, Y., 2019, "DLC and Glycerol: Superlubricity in Rolling/Sliding Elastohydrodynamic Lubrication," Tribology Letters, **67**(1).

[2] Sheeja, D., Tay, B. K., Krishnan, S. M., and Nung, L. N., 2003, "Tribological Characterization of Diamond-like Carbon (DLC) Coatings Sliding against DLC Coatings," Diamond and Related Materials, **12**(8), pp. 1389–1395.

[3] Evans, R. D., Cogdell, J. D., and Richter, G. A., 2009, "Traction of Lubricated Rolling Contacts between Thin-Film Coatings and Steel," Tribology Transactions, **52**(1), pp. 106–113.

[4] Katsaros, K., Bompos, D. A., Nikolakopoulos, P. G., and Theodossiades, S., 2018, "Thermal-Hydrodynamic Behaviour of Coated Pivoted Pad Thrust Bearings: Comparison between Babbitt, PTFE and DLC," Lubricants, **6**(2), pp. 0–18.

[5] Wu, L. Y. L., Ngian, S. K., Chen, Z., and Xuan, D. T. T., 2011, "Quantitative Test Method for Evaluation of Anti-Fingerprint Property of Coated Surfaces," Applied Surface Science, **257**(7), pp. 2965–2969.

[6] Meng, X., Wang, J., Nishikawa, H., and Nagayama, G., 2021, "Effects of Boundary Slips on Thermal Elastohydrodynamic Lubrication under Pure Rolling and Opposite Sliding Contacts," Tribology International, **155**, p. 106801.

[7] Thompson, P. A., and Troian, S. M., 1997, "A General Boundary Condition for Liquid Flow at Solid Surfaces," Nature, **389**(6649), pp. 360–362.

[8] Neto, C., Evans, D. R., Bonaccurso, E., Butt, H. J., and Craig, V. S. J., 2005, "Boundary Slip in Newtonian Liquids: A Review of Experimental Studies," Reports on Progress in Physics, **68**(12), pp. 2859–2897.

[9] Kapitza, P. L., 1971, "The Study of Heat Transfer in Helium II," *Helium 4*, pp. 114–153.

[10] Pollack, G. L., 1969, "Kapitza Resistance," Reviews of Modern Physics, **41**(1), pp. 48–

81.

[11] Nagayama, G., 2011, “Boundary Conditions and Microscale Heat Transfer at Solid-Liquid Interface,” Journal of the Heat Transfer Society of Japan, **50**(211), pp. 29–36.

[12] Kaneta, M., Nishikawa, H., and Kameishi, K., 1990, “Observation of Wall Slip in Elastohydrodynamic Lubrication,” Journal of Tribology, **112**(3), pp. 447–452.

[13] Ehret, P., and Bauget, F., 2001, “Observation of Kaneta’s Dimples in Elastohydrodynamic Lubrication Contacts,” Proceedings of the Institution of Mechanical Engineers, Part J: Journal of Engineering Tribology, **215**(3), pp. 289–300.

[14] Fu, Z., Guo, F., and Wong, P. L., 2007, “Non-Classical Elastohydrodynamic Lubricating Film Shape under Large Slide-Roll Ratios,” Tribology Letters, **27**(2), pp. 211–219.

[15] Kalin, M., Velkavrh, I., and Vižintin, J., 2009, “The Stribeck Curve and Lubrication Design for Non-Fully Wetted Surfaces,” Wear, **267**(5), pp. 1232–1240.

[16] Guo, F., Li, X. M., and Wong, P. L., 2012, “A Novel Approach to Measures Slip-Length of Thin Lubricant Films under High Pressures,” Tribology International, **46**(1), pp. 22–29.

[17] Guo, F., and Wong, P. L., 2016, “An Anomalous Elastohydrodynamic Lubrication Film: Inlet Dimple,” Journal of Tribology, **127**(2), pp. 425–434.

[18] Guo, F., and Wong, P. L., 2004, “Experimental Observation of a Dimple-Wedge Elastohydrodynamic Lubricating Film,” Tribology International, **37**(2), pp. 119–127.

[19] Ponjavic, A., Chennaoui, M., and Wong, J. S. S., 2013, “Through-Thickness Velocity Profile Measurements in an Elastohydrodynamic Contact,” Tribology Letters, **50**(2), pp. 261–277.

[20] Ponjavic, A., and Wong, J. S. S., 2014, “The Effect of Boundary Slip on Elastohydrodynamic Lubrication,” RSC Advances, **4**(40), pp. 20821–20829.

[21] Wang, P., and Reddyhoff, T., 2017, “Wall Slip in an EHL Contact Lubricated with 1-

Dodecanol," Tribology International, **113**, pp. 197–205.

[22] Zhao, Y., Wong, P. L., and Mao, J. H., 2018, "EHL Film Formation under Zero Entrainment Velocity Condition," Tribology International, **124**, pp. 1–9.

[23] Wong, P. L., Zhao, Y., and Mao, J., 2018, "Facilitating Effective Hydrodynamic Lubrication for Zero-Entrainment-Velocity Contacts Based on Boundary Slip Mechanism," Tribology International, **128**, pp. 89–95.

[24] Wen, S., and Zhang, Y., 2000, "EHL Performance of the Lubricant With Shear Strength: Part I — Boundary Slippage and Film Failure," Tribology Transactions, **43**(4), pp. 700–710.

[25] Ståhl, J., and Jacobson, B. O., 2003, "A Lubricant Model Considering Wall-Slip in EHL Line Contacts," Journal of Tribology, **125**(3), pp. 523–532.

[26] Chu, L. M., Lin, J. R., Li, W. L., and Lu, J. M., 2012, "A Model for Line-Contact EHL Problems-Consideration of Effects of Navier-Slip and Lubricant Rheology," Journal of Tribology, **134(3)**.

[27] Chen, Q. Da, Jao, H. C., Chu, L. M., and Li, W. L., 2016, "Effects of Anisotropic Slip on the Elastohydrodynamic Lubrication of Circular Contacts," Journal of Tribology, **138**(3), pp. 1–48.

[28] Cheng, H. S., 1965, "A Refined Solution to the Thermal-Elastohydrodynamic Lubrication of Rolling and Sliding Cylinders," ASLE Transactions, **8**(4), pp. 397–410.

[29] Guo, F., Yang, P., and Qu, S., 2001, "On the Theory of Thermal Elastohydrodynamic Lubrication at High Slide-Roll Ratios - Circular Glass-Steel Contact Solution at Opposite Sliding," Journal of Tribology, **123**(4), pp. 816–821.

[30] Yagi, K., Kyogoku, K., and Nakahara, T., 2006, "Experimental Investigation of Effects of Slip Ratio on Elastohydrodynamic Lubrication Film Related to Temperature Distribution in Oil Films," Proceedings of the Institution of Mechanical Engineers, Part

J: Journal of Engineering Tribology, **220**(4), pp. 353–363.

[31] Wang, J., and Yang, P., 2003, “A Numerical Analysis for TEHL of Eccentric-Tappet Pair Subjected to Transient Load,” Journal of Tribology, **125**(4), pp. 770–779.

[32] Zhao, Y., Wong, P. L., and Mao, J. H., 2019, “Solving Coupled Boundary Slip and Heat Transfer EHL Problem under Large Slide–Roll Ratio Conditions,” Tribology International, **133**, pp. 73–87.

[33] Zhang, Y., Wang, W., Liang, H., and Zhao, Z., 2020, “Slip Status in Lubricated Point-Contact Based on Layered Oil Slip Lubrication Model,” Tribology International, **144**(September 2019), p. 106104.

[34] Zhang, Y., Wang, W., Liang, H., and Zhao, Z., 2019, “Layered Oil Slip Model for Investigation of Film Thickness Behaviours at High Speed Conditions,” Tribology International, **131**(August 2018), pp. 137–147.

[35] Ge, Z., Cahill, D. G., and Braun, P. V., 2006, “Thermal Conductance of Hydrophilic and Hydrophobic Interfaces,” Physical Review Letters, **96**(18), pp. 1–4.

[36] Timofeeva, E. V., Smith, D. S., Yu, W., France, D. M., Singh, D., and Routbort, J. L., 2010, “Particle Size and Interfacial Effects on Thermo-Physical and Heat Transfer Characteristics of Water-Based α-SiC Nanofluids,” Nanotechnology, **21**, p. 215703.

[37] Nagayama, G., Matsumoto, T., Fukushima, K., and Tsuruta, T., 2017, “Scale Effect of Slip Boundary Condition at Solid-Liquid Interface,” Scientific Reports, **7**, pp. 1–8.

[38] Nagayama, G., Kawagoe, M., Tokunaga, A., and Tsuruta, T., 2010, “On the Evaporation Rate of Ultra-Thin Liquid Film at the Nanostructured Surface: A Molecular Dynamics Study,” International Journal of Thermal Sciences, **49**(1), pp. 59–66.

[39] Hu, H., and Sun, Y., 2012, “Effect of Nanopatterns on Kapitza Resistance at a Water-Gold Interface during Boiling: A Molecular Dynamics Study,” Journal of Applied Physics, **112**(5), p. 053508.

[40] Shi, Z., Barisik, M., and Beskok, A., 2012, “Molecular Dynamics Modeling of Thermal Resistance at Argon-Graphite and Argon-Silver Interfaces,” International Journal of Thermal Sciences, **59**, pp. 29–37.

[41] Barisik, M., and Beskok, A., 2014, “Temperature Dependence of Thermal Resistance at the Water/Silicon Interface,” International Journal of Thermal Sciences, **77**, pp. 47–54.

[42] Pham, A. T., Barisik, M., and Kim, B. H., 2016, “Interfacial Thermal Resistance between the Graphene-Coated Copper and Liquid Water,” International Journal of Heat and Mass Transfer, **97**, pp. 422–431.

[43] Song, Z., Cui, Z., Cao, Q., Liu, Y., and Li, J., 2021, “Molecular Dynamics Study of Convective Heat Transfer in Ordered Rough Nanochannels,” Journal of Molecular Liquids, **337**, p. 116052.

[44] Peiran, Y., and Shizhu, W., 1990, “A Generalized Reynolds Equation Based on Non-Newtonian Flow in Lubrication Mechanics,” Acta Mechanica Sinica, **6**(4), pp. 289–295.

[45] Yang, P., 1998, *Numerical Analysis of Fluid Lubrication*, National Defense Industry Press.

[46] Dowson, D., and Higginson, G. R., 1977, *Elasto-hydrodynamic Theory*.

[47] Roelands, C. J. A., Winer, W. O., and Wright, W. A., 1971, “Correlational Aspects of the Viscosity-Temperature-Pressure Relationship of Lubricating Oils,” Journal of Lubrication Technology.

[48] Habchi, W., and Bair, S., 2020, “The Role of the Thermal Conductivity of Steel in Quantitative Elastohydrodynamic Friction,” Tribology International, **142**, p. 105970.

[49] Reddyhoff, T., Schmidt, A., and Spikes, H., 2019, “Thermal Conductivity and Flash Temperature,” Tribology Letters, **67**(22).

[50] Liu, H. C., Zhang, B. B., Bader, N., Poll, G., and Venner, C. H., 2020, “Influences of Solid and Lubricant Thermal Conductivity on Traction in an EHL Circular Contact,”

Tribology International, **146**(2), p. 106059.

[51] Venner, C. H., and Lubrecht, A. A., 2000, *Multilevel Methods in Lubrication*.

[52] Yang, P., and Rodkiewicz, C. M., 1997, "On the Numerical Analysis to the Thermoelastohydrodynamic Lubrication of a Tilting Pad Inclusive of Side Leakage," Tribology Transactions, **40**(2), pp. 259–266.

[53] Hamrock, B. J., and Dowson, D., 1981, *Ball Bearing Lubrication. The Elastohydrodynamics of Elliptical Contacts.*

[54] Savio, D., Fillot, N., Vergne, P., Hetzler, H., Seemann, W., and Morales Espejel, G. E., 2015, "A Multiscale Study on the Wall Slip Effect in a Ceramic-Steel Contact with Nanometer-Thick Lubricant Film by a Nano-to-Elastohydrodynamic Lubrication Approach," Journal of Tribology, **137(3)**.

[55] Nagayama, G., and Cheng, P., 2004, "Effects of Interface Wettability on Microscale Flow by Molecular Dynamics Simulation," International Journal of Heat and Mass Transfer, **47**(3), pp. 501–513.

[56] Björling, M., Habchi, W., Bair, S., Larsson, R., and Marklund, P., 2014, "Friction Reduction in Elastohydrodynamic Contacts by Thin-Layer Thermal Insulation," Tribology Letters, **53**(2), pp. 477–486.

Figure Captions List

Fig. 1 Schematic illustrations of (a) sliding/rolling contact, and (b) computational domain (not to scale)

Fig. 2 Boundary slips at surfaces of moving solids: velocity slip (left) and thermal slip (right)

Fig. 3 Contour maps of film thickness (top) and pressure, film thickness profiles on center plane $Y = 0$ (bottom) at $u_e = 3.6$ m/s, SRR = 1.5 under different boundary conditions: (a) no slip; (b) velocity slip; (c) thermal slip; (d) coupled velocity/thermal slips. Dotted line represents minimum film thickness of no-slip case; dashed line represents minimum film thickness for case of $l_s = l_k = 0.2$ μm

Fig. 4 Temperature profiles on center plane ($Y = 0$) in EHL contact area at $u_e = 3.6$ m/s, SRR = 1.5 under different boundary conditions: (a) $l_s = l_k = 0$; (b) $l_s = 0.2$ μm, $l_k = 0$; (c) $l_s = 0$, $l_k = 0.2$ μm; (d) $l_s = l_k = 0.2$ μm. Dotted line represents minimum film thickness of (a); dashed line represents minimum film thickness of (d)

Fig. 5 Contour maps of film thickness (top) and pressure. Film profiles on center plane $Y = 0$ (bottom) at $u_e = 3.6$ m/s, SRR = 1.5 under coupled velocity/thermal slips: (a) $l_s / l_k = 0.1$ μm/ 0.5 μm; (b) $l_s / l_k = 0.1$ μm/ 5.0 μm; (c) $l_s / l_k = 0.1$ μm/ 50.0 μm; (d) $l_s / l_k = 0.5$ μm/ 0.1 μm; (e) $l_s / l_k = 5.0$ μm/ 0.1 μm

Fig. 6 Temperature profiles in EHL contact area on center plane $Y = 0$ at $u_e = 3.6$ m/s and SRR = 1.5 under coupled velocity/thermal slips: (a) $l_s / l_k = 0.1$ μm/ 0.5 μm; (b) $l_s / l_k = 0.1$ μm/ 5.0 μm; (c) $l_s / l_k = 0.1$ μm/ 50.0 μm; (d) $l_s / l_k = 0.5$ μm/ 0.1 μm; (e) $l_s / l_k = 5.0$ μm/ 0.1 μm

Fig. 7 Effect of entrainment velocity on lubrication performance at SRR = 1.5: (a) minimum film thickness; (b) mean lubricant temperature rise in entire contact area. Dashed line corresponds to u_e = 3.6 m/s applied in Figs. 3–4

Fig. 8 Reduction ratio of minimum film thickness ε vs. entrainment velocity curves at SRR = 1.5. Dashed line represents threshold between regions *I* and *II*

Fig. 9 Friction coefficient vs. SRR curves at u_e = 3.6 m/s

Fig. 10 Friction coefficient vs. SRR curves at u_e = 3.6 m/s

Fig. 11 Comparisons of *f*-SRR curve between experiments [1] and numerical simulations at u_e = 1.6 m/s and *w* = 300 N

Table Caption List